

SANDIA REPORT

SAND2014-19826

Unlimited Release

Printed November 2014

Low-Cost Spectral Sensor Development Description

Kenneth M. Armijo and Julius Yellowhair

Prepared by
Sandia National Laboratories
Albuquerque, New Mexico 87185 and Livermore, California 94550

Sandia National Laboratories is a multi-program laboratory managed and operated by Sandia Corporation, a wholly owned subsidiary of Lockheed Martin Corporation, for the U.S. Department of Energy's National Nuclear Security Administration under contract DE-AC04-94AL85000.

Approved for public release; further dissemination unlimited.



Sandia National Laboratories

Issued by Sandia National Laboratories, operated for the United States Department of Energy by Sandia Corporation.

NOTICE: This report was prepared as an account of work sponsored by an agency of the United States Government. Neither the United States Government, nor any agency thereof, nor any of their employees, nor any of their contractors, subcontractors, or their employees, make any warranty, express or implied, or assume any legal liability or responsibility for the accuracy, completeness, or usefulness of any information, apparatus, product, or process disclosed, or represent that its use would not infringe privately owned rights. Reference herein to any specific commercial product, process, or service by trade name, trademark, manufacturer, or otherwise, does not necessarily constitute or imply its endorsement, recommendation, or favoring by the United States Government, any agency thereof, or any of their contractors or subcontractors. The views and opinions expressed herein do not necessarily state or reflect those of the United States Government, any agency thereof, or any of their contractors.

Printed in the United States of America. This report has been reproduced directly from the best available copy.

Available to DOE and DOE contractors from

U.S. Department of Energy
Office of Scientific and Technical Information
P.O. Box 62
Oak Ridge, TN 37831

Telephone: (865) 576-8401
Facsimile: (865) 576-5728
E-Mail: reports@osti.gov
Online ordering: <http://www.osti.gov/scitech>

Available to the public from

U.S. Department of Commerce
National Technical Information Service
5301 Shawnee Rd
Alexandria, VA 22312

Telephone: (800) 553-6847
Facsimile: (703) 605-6900
E-Mail: orders@ntis.gov
Online order: <http://www.ntis.gov/search>



Low-Cost Spectral Sensor Development Description

Kenneth M. Armijo
Photovoltaic and Distributed Systems
Integration Department
Sandia National Laboratories
P.O. Box 5800
Albuquerque, New Mexico 87185-MS0951

Julius Yellowhair
Concentrating Solar Technologies Department
Sandia National Laboratories
P.O. Box 5800
Albuquerque, New Mexico 87185-MS1127

Abstract

Solar spectral data for all parts of the US is limited due in part to the high cost of commercial spectrometers. Solar spectral information is necessary for accurate photovoltaic (PV) performance forecasting, especially for large utility-scale PV installations. A low-cost solar spectral sensor would address the obstacles and needs. In this report, a novel low-cost, discrete-band sensor device, comprised of five narrow-band sensors, is described. The hardware is comprised of commercial-off-the-shelf components to keep the cost low. Data processing algorithms were developed and are being refined for robustness. PV module short-circuit current (I_{sc}) prediction methods were developed based on interaction-terms regression methodology and spectrum reconstruction methodology for computing I_{sc} . The results suggest the computed spectrum using the reconstruction method agreed well with the measured spectrum from the wide-band spectrometer (RMS error of 38.2 W/m²-nm). Further analysis of computed I_{sc} found a close correspondence of 0.05 A RMS error. The goal is for ubiquitous adoption of the low-cost spectral sensor in solar PV and other applications such as weather forecasting.

ACKNOWLEDGMENTS

Sandia National Laboratories is a multi-program laboratory managed and operated by Sandia Corporation, a wholly owned subsidiary of Lockheed Martin Corporation, for the U.S. Department of Energy's National Nuclear Security Administration under contract DE-AC04-94AL85000. This work was primarily funded by the US Department of Energy Solar Energy Technologies Program. This material is also based upon work partially supported by the U.S. Department of Homeland Security under Grant Award Numbers 2012-DN-130-NF0001-0202 and HSHQDC12X00059. The views and conclusions contained in this document are those of the authors and should not be interpreted as representing the official policies, either expressed or implied, of the U.S. Department of Homeland Security. The authors would also like to acknowledge fundamental contributions from Dr. Richard K. Harrison who is a staff scientist at Sandia National Laboratories.

CONTENTS

1. Introduction.....	9
2. Methodology.....	11
2.1. Preliminary Studies.....	12
2.2. Hardware.....	16
2.3. Software and Data Processing	18
3. Results.....	22
4. Conclusions.....	28
5. References.....	30
Appendix A: Silicon Photodiodes	32
Appendix B: Spectral Bandpass Filters	34

FIGURES

Figure 1. Variation of the relative in-band solar irradiance over a clear day during Oct. 2013 (top), and the variations within the narrow spectral bands (bottom)	13
Figure 2. Measured versus semi-empirically determined I_{sc} (in-band) analysis for morning and afternoon periods on Oct. 5 th , 2013, for a m-Si flat panel module	14
Figure 3. Morning versus afternoon average difference analysis against water absorption bands for a clear-sky day and an m-Si flat panel module	14
Figure 4. Calculated transmission spectra using SMARTS2 for Albuquerque, NM at solar noon, for six different atmospheric radiative forcing components.....	16
Figure 5. (a) Image of the prototype low-cost spectral sensor with the portable DAQ system. The sixth sensor is a floating sensor that can be used to further reduce the uncertainty in the measurements and calculations. (b) Prototype low-cost spectrometer assembly containing five narrow-band sensors, located next to the weather station on the two-axis tracker at the Sandia PSEL site..	17
Figure 6. Regression between measured and predicted m-Si module I_{sc} using a regression method with seasonal interaction terms. The blue line provides a one-to-one correspondence reference while the red points are the respective data values for the five months..	19
Figure 7. Solar spectral irradiance prediction model comparison with the measured c-Si module data.....	20
Figure 8. Photodiodes Gain Setting Optimization Analysis for the 630nm sensor.	22

Figure 9. Photodiodes Sensor Calibration Analysis for the 630 nm and 940 nm sensors.	23
Figure 10. Calibrated photodiode measurements (red) of 500nm 580nm 630nm and 940nm bands, with EKO spectrometer data (blue).	23
Figure 11. (a) Extraterrestrial and global tilt spectral irradiance (ASTM G-173). A ratio of the two curves in (a) provides the (b) transmittance through the atmosphere (from extraterrestrial to the ground).	24
Figure 12. (a) Extraterrestrial spectral irradiance compared to the measured spectral irradiance at 11:40 am local time on Oct. 1, 2014 in Albuquerque, NM, and the data from the calibrated spectral sensors (red dots) for the same day and time. (b) Transmittance profile of the measured spectral irradiance shown in (a) and the corresponding calculated transmittance from the PD spectral sensors (red dots). Note that the r2 factor was not accounted for in the calculation.	25
Figure 13. Calculated spectrum based on discrete photodiode measurements and computation within the Sandia Spectral Transmission Model, compared with measured full-band spectrum from an EKO spectrometer for October 1, 2014.	25
Figure 14. Comparison of short circuit current between EKO spectrometer and measured photodiode data with spectral reconstruction using the Sandia Spectral Transmission Model, for October 1, 2014.	26

TABLES

Table 1. Current market low-cost spectrometer suppliers including the SNL prototype cost.	10
Table 2. Selected spectral bands for the low-cost sensor development.	15
Table 3. Parts list, including cost, to build the prototype spectral sensor.	17

NOMENCLATURE

I_{sc}	short circuit current
c-Si	crystalline silicon
m-Si	monolithic silicon
PSEL	Photovoltaic Solar Evaluation Laboratory
DAQ	data acquisition system
T_{cell}	cell temperature
SR	spectral response
SI	spectral irradiance
A_{cell}	cell active area
Calc	calculated
E	irradiance
E_0	extra-terrestrial irradiance
r	earth sun distance
T_a	aerosols transmission
T_g	mixed gases transmission
T_n	nitrogen dioxide transmission
T_o	ozone transmission
T_R	Raleigh transmission
T_w	water transmission
λ	wavelength

1. INTRODUCTION

Site selection can have a large impact on the return on investment (ROI) for planned utility-scale photovoltaic (PV) plants. Site-specific solar spectrum must be considered to optimally utilize solar resources at a given location. Decisions can then be made pertaining to the appropriate solar technology to optimize power generation for a respective site, which in turn has a positive impact on ROI. The rise of commercially relevant non-silicon thin film photovoltaic materials, such as CIGS (copper indium gallium selenide) and CdTe (cadmium telluride), provides utilization of many traditionally-underutilized energy bandgaps that can be optimized for local solar spectra. These can be more red- or blue-shifted compared to the ASTM G-173 standard. In addition, spectral ratios (specific spectral bands compared to the ASTM G-173 standard) may vary between locations. These spectral variations can also impact multi-junction PV cells by shifting the current-limiting junction. After an appropriate PV technology is selected for a site, daily solar spectrum must be monitored to accurately predict performance for a PV plant, where inaccuracies in predicting plant performance have direct impacts on levelized cost of energy (LCOE) and financial returns. Variability in solar spectrum between locations with different climatic environments can be due to differences in atmospheric components that reflect, absorb, and/or scatter incident sunlight. Specific geographically-varying atmospheric components like water vapor and aerosols can have appreciable impacts on the spectrum that ideally should be accounted for. Unfortunately, instruments that measure solar spectrum (i.e. spectrometers) are often expensive, delicate, or relegated to laboratory use. Spectrometers rated for outdoor environments are even more expensive (~\$100k), making it cost prohibitive for most PV plants. Table 1 lists current commercially available solar spectral sensors and the prototype spectral sensor Sandia National Laboratories (SNL) is developing. Two of these devices cover a wavelength range that is sufficient to measure a good portion of the solar spectrum that encompasses the response range of most PV cells, while three have a limited wavelength range (cut-off at 1000 nm or less). Of the two that are sufficient, one is suitable for outdoor use; the other is for indoor use only. However, the one that is suitable for outdoor use is cost prohibitive (>\$60k). Thus, a need exists for a low-cost device suitable for outdoor use that can provide enough spectral information for PV predictive models, which accurately accounts for atmospheric components present along the atmospheric path of incident sunlight.

Current commercial solar photometers, such as the [Cimel Multiband Photometer CE318](#) and the [Solarlight Microtops II](#), using similar sensing approaches are relatively expensive, require tracking, and are designed based on aerosol measurements rather than with sunlight spectral quality, important for accurate PV current generation predictions. The comparison of a limited number of specific spectral ratios has also been used in satellite observation research to extract historical atmospheric transmission data. However, key resultant differences would be an inexpensive device that is robust that provides the desired information about preferred solar technology for a given location.

Table 1. Current market low-cost spectrometer suppliers including the SNL prototype cost.

Spectrometer Model	Manufacturer / Vendor	Measurement Wavelength Range (nm)	Listed Cost
CXR-SR Super Range Spectrometer	StellarNet, Inc.	220 – 1100	\$ 3,459
FieldSpec 4	ASD, Inc.	350 – 2500	\$ 64,347
PS-100	Apogee	350 – 1000	\$ 4,395
ACC-VIS	Ramses	320 – 950	\$ 8,378
SP-75	CSA Group / ORB Optronix	250 – 1000	\$ 4,320
Discrete Bands Spectrometer Unit (prototype)	Sandia National Laboratories	480-520, 625-635, 775-785, 935-945, 1045-1055	\$ 1,121*

* This cost is to build one prototype system, which does not include costs of insurance, capital, servicing/warranty, advertising and profit. If manufactured, this cost will be reduced.

For this research, Sandia is developing a low-cost spectral sensing device that monitors specific narrow bands of the solar spectrum to reconstruct the entire solar spectrum and estimate the PV module short-circuit current directly. These will be accomplished by analysis consideration of the main attenuating atmospheric components (e.g. H₂O, O₃, aerosols, etc.). Commercial-off-the-shelf components were used to construct the spectral sensor to keep the cost low. In this report an overview is presented for a novel method for determination of discrete spectral bands for accurate PV power forecasting, and the development of the low-cost spectral sensor prototype. Also described is the development of the algorithms needed for post-processing of sensor data.

2. METHODOLOGY

2.1. Preliminary Studies

In this work, the Sandia team retrieved outdoor spectroradiometer data to analyze daily variations in spectral irradiance levels over varying spectral bandwidths. Next the development of a computational model in Matlab was performed to evaluate this data along with localized weather station and electrical performance data of crystalline silicon (c-Si) flat-plate PV modules that were mounted on a two-axis tracker during this same time period. Our study investigated the short-circuit current and air mass variability between mornings and afternoons, and evaluated the hysteresis correlation between them and their variability at specific spectral regions. After gaining a better understanding of the correlations, we identified five to six specific narrow spectral bands for our low-cost spectral sensor development. To accomplish this, six bands were selected based on the following criteria:

1. Surrogate bands based on relative normalized I_{sc}
2. Stable spectrum bands
3. Aerosol particulate bands
4. Highly attenuating water bands
5. Ozone and other bands with low spectral variability.

In the initial studies, narrow band spectral impacts on measured I_{sc} were studied to investigate potential causes of morning/afternoon differences in relative normalized I_{sc} , and thus attempt to improve PV prediction models. From our spectroradiometer data for three clear-sky days in October 2013, we investigated spectrum variations over narrow bands at AM1.5 to understand the impacts on the measured I_{sc} . We found that the narrow spectrums varied more in the morning at shorter wavelengths (400-500nm) and over the water absorption bands. The analysis (for three days in one month) showed aerosols and water content in the atmosphere affect the spectrum in the morning more than in the afternoon for Albuquerque, NM. Further comparison of morning and afternoon spectrums showed higher transmissions at the shorter wavelengths (400-500nm) and water absorption bands in the afternoon. Therefore, the measured I_{sc} might be higher in the afternoon at AM1.5 than in the morning. For the low-cost sensor development, the spectral regions that show large difference between morning and afternoon were of interest.

The top plot in Figure 1 shows the relative in-band irradiances (over 10 nm wavebands) for different air masses in the morning and afternoon on October 05, 2013. The lower plot shows the standard deviations over the 10 nm wide wavebands, which reveals the variations over the narrow wavebands throughout the course of the day. The spectral waveband least affected by the atmosphere is around 630 nm, which we determined also provides an overall good proxy for I_{sc} measured over the course of the day. The high variations in the shorter wavelengths are caused by aerosols. Particulates and aerosols also affect the spectrum at higher wavelengths. The results of this analysis were based on data from a few clear days in October 2013. We plan to extend and repeat the analysis for other months to study monthly and seasonal variations.

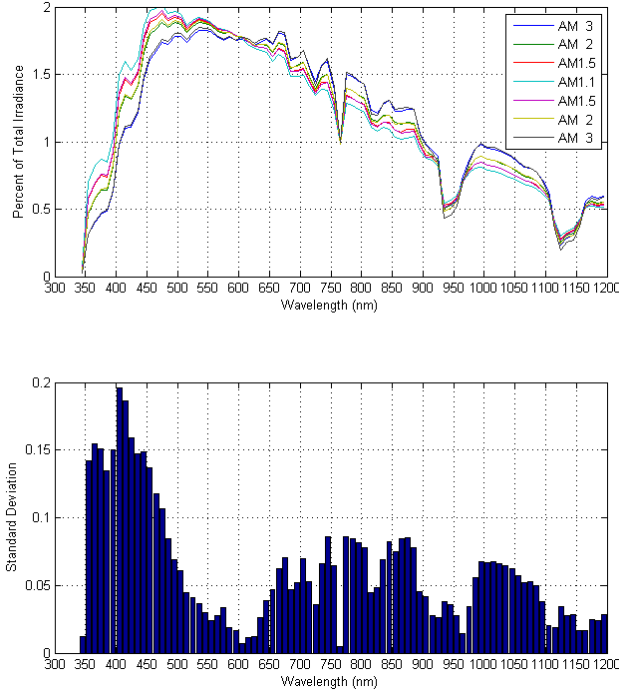


Figure 1. Variation of the relative in-band solar irradiance over a clear day during Oct. 2013 (top), and the variations within the narrow spectral bands (bottom).

From our spectral analysis described above, we determined two narrow spectral bands that could serve as proxies for the I_{sc} of a monocrystalline silicon (m-Si) module. We calculated the equivalent short-circuit current from the narrow spectral bands and compared them to the I_{sc} distribution over the course of the day. The results suggest that $I_{sc-inband}$ from the bands around 620 and 965 nm closely matched (in form) the measured I_{sc} directly from the device, as shown in Figure 2. Further investigation also revealed that the 965 nm band provided a closer surrogate match to measured I_{sc} during the morning, while the 620 nm band provided a closer surrogate during the afternoon. This suggests that atmospheric component concentration variations (i.e. H_2O , aerosols) throughout the day may have a direct correspondence to PV module power generation. These two surrogate spectral bands were considered for the low-cost sensor development.

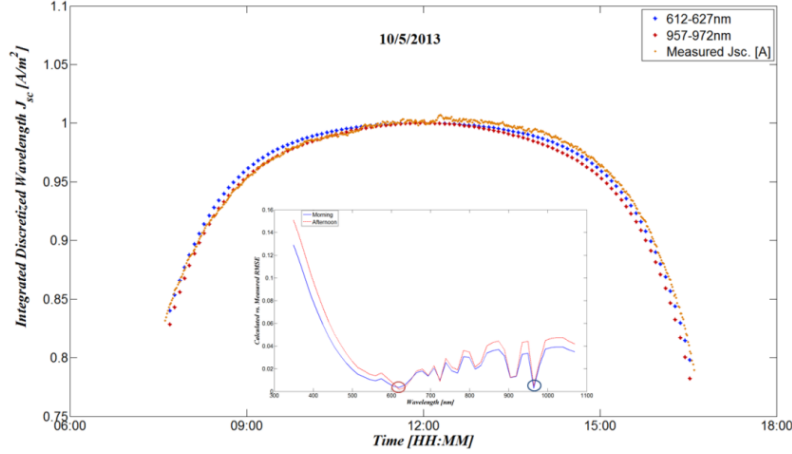


Figure 2. Measured versus semi-empirically determined I_{sc} (in-band) analysis for morning and afternoon periods on Oct. 5th, 2013, for a m-Si flat panel module.

Further analysis between morning and afternoon average differences and the water absorption bands, in Figure 3, shows a strong correspondence between high AM/PM variations and the water absorption bands. These results suggest that much of the variability in measured I_{sc} and air mass could be due to daily concentration variability in atmospheric components such as precipitable water which impacts light attenuation and absorption levels. Although these results are presented for one day during autumn environmental conditions, other results during summer conditions suggest similar correspondence between AM/PM variability and specific water absorption portions of the spectrum for m-Si.

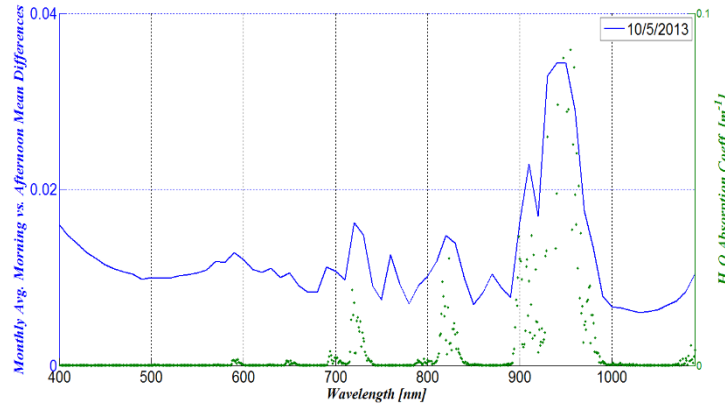


Figure 3. Morning versus afternoon average difference analysis against water absorption bands for a clear-sky day and an m-Si flat panel module.

Absorption bands for ozone and other atmospheric gasses were not shown to have large impacts on the solar spectrum throughout the course of the day. Further corroboration of this result can be found in [1], where the investigators only found a 0.07%/cmO₃ change in module energy generation. In our low-cost sensor development we limited to the number of spectral bands to five, since the addition of spectral bands would increase the cost of the device. For this

reason ozone and atmospheric gasses will not be monitored with the initial spectral sensor prototype.

From this analysis, the bands chosen for study are listed in Table 2, and their respective justifications for selection. Spectral bands were chosen based on their relative capabilities for approximating spectrum, having relative stability and their sensitivity to highly attenuating atmospheric component concentration variations. However, these spectral bands may be refined as work progresses with sensor development and PV derate research.

Table 2. Selected spectral bands for the low-cost sensor development.

Spectral Band (nm)	Rationale for Selection
480-520	Large variations in the spectrum caused by aerosols and particulates
625-635	Provides a good proxy for I_{sc} and is stable against atmospheric changes
775-785	Variations in the spectrum caused by aerosols and particulates
935-945	Largest H ₂ O absorption band, and provides good proxy for device I_{sc} .
1045-1055	Relative stability near the large water absorption bands

Shown in Figure 4 is the calculated transmission spectra for Albuquerque, NM at solar noon using the SMARTS atmospheric modeling tool. As suggested above the transmission spectra of water vapor has the highest attenuation compared to other atmospheric components.

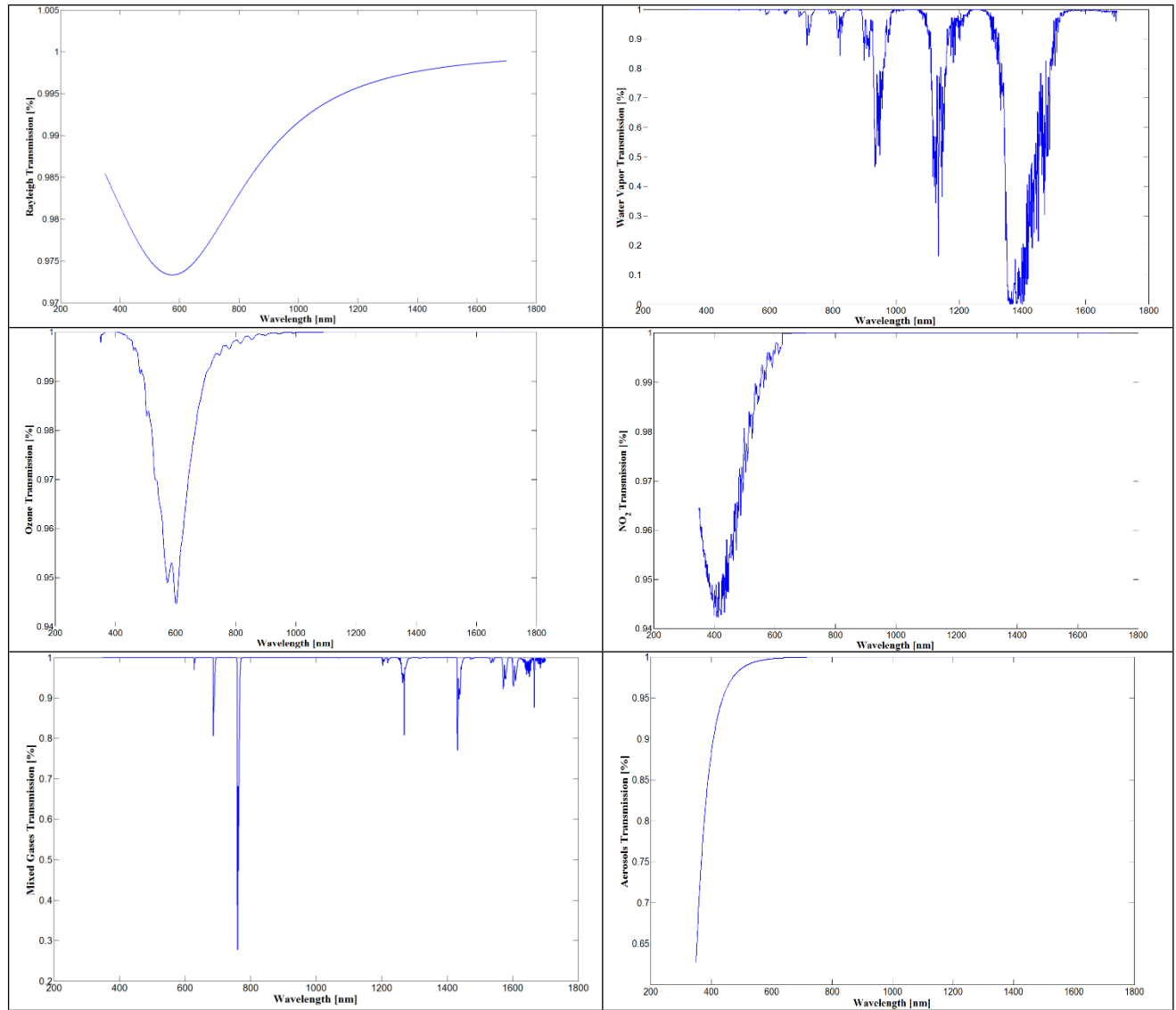


Figure 4. Calculated transmission spectra using SMARTS2 for Albuquerque, NM at solar noon, for six different atmospheric radiative forcing components.

2.2. Hardware

For the first low-cost spectrometer prototype, the Sandia team developed a sensor package requiring a two-axis tracker and a connected outdoor-adapted data acquisition (DAQ) system. The prototype design was finalized, which included six silicon photodiodes, six narrow band filters and optical mounting hardware. These components were purchased to build a proof-of concept, bread-board module for preliminary testing. An image of the sensor package is shown in Figure 5. The components used to build the device are commercial-off-the-shelf parts listed in Table 3 with their respective prototype costs. This sensor assembly required alignment calibration, and is currently installed on the Sandia PSEL weather station two-axis tracker (see

Figure 4b) next to a full-band EKO spectrometer. A second generation system is currently being built with a design that requires custom parts, but at a fraction of the cost of prototype 1. The DAQ system used during the tests consisted of a logicbeach data logger, which required calibration and gain settings optimization for each respective photodiode/filter pair. Data was collected clear-sky periods in 1-minute increments each day of testing.

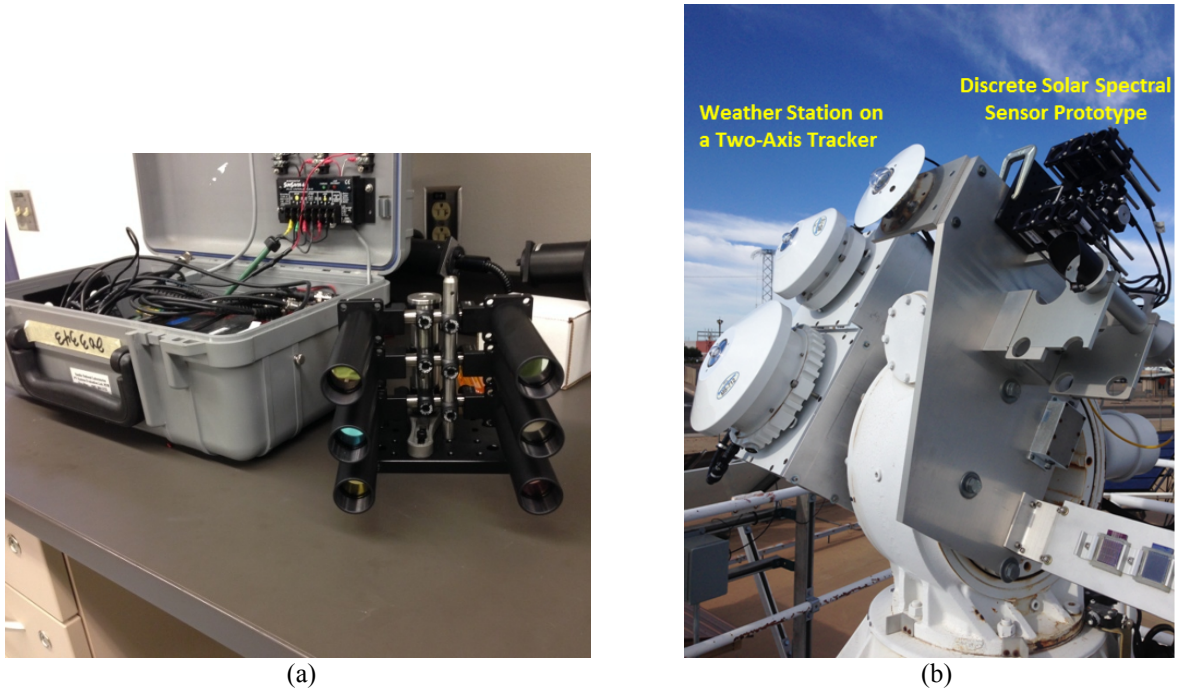


Figure 5. (a) Image of the prototype low-cost spectral sensor with the portable DAQ system. The sixth sensor is a floating sensor that can be used to further reduce the uncertainty in the measurements and calculations. (b) Prototype low-cost spectrometer assembly containing five narrow-band sensors, located next to the weather station on the two-axis tracker at the Sandia PSEL site.

Table 3. Parts list, including cost, to build the prototype spectral sensor.

Part / Item	Manufacturer / Vendor	Part Number	Cost
Silicon photodiodes, 10mm x 10mm (x 5)	Thorlabs	FDS10x10	\$ 244
Bandpass filters, 1" diameter (x 5)	Thorlabs	FB500-40 FB630-10 FB780-10 FB940-10 FB1050-10	\$ 456
Misc hardware & electrical wiring/connectors	Thorlabs, Edmund Optics, and Digikey	---	\$ 421
TOTAL COST			\$ 1,121

2.3. Software and Data Processing

Our low-cost sensor development approach measures the solar spectrum at discrete spectral bands, which are listed in Table 2. These spectral bands were determined from the spectral analysis study; the spectral bands may be refined as the sensor development progresses. For the surrogate analysis study, temperature-corrected measured I_{sc} values for a m-Si flat-panel module, and semi-empirical short circuit current data band was determined based on Eqns. 1 and 2.

$$I_{sc, Meas Temp. Corrected} = \frac{I_{sc, Meas}}{1 + \alpha_{Th} (T_{cell} - 25)} \quad (1)$$

$$I_{sc, Calc} = A_{cell} \int_{\lambda_1}^{\lambda_2} SR_{m-Si} \cdot SI_{Meas} d\lambda \quad (2)$$

From the analysis, as presented in Figure 2, over a clear-sky day period (DNI/GNI>0.9) in Oct. 2103, the observed data suggests good correspondence between measured J_{sc} data and calculated J_{sc} two spectral bands.

To reduce the uncertainty in the solar spectrum data and module short-circuit current predictions, two methods were developed for post-processing of the sensor data. The goal was to develop a truly low-cost spectrometer that has unmatched performance. The first method takes the data from the five sensors and directly predict the short-circuit current of the m-Si PV module by developing advanced statistical methods that included regressions and interaction coefficient analysis. Figure 6 shows an example of the results of this method. The directly measured I_{sc} from m-Si modules are compared to the calculated I_{sc} from regressions, which includes interaction coefficients over five months during 2013. The interaction coefficients must be optimized for seasonal (and daily) variations of solar spectrum. These preliminary results suggest good correlation between calculated and measured I_{sc} for all months, except February where a small deviation was observed. The proxy spectral bands for the module short-circuit current (second method) can then be used to verify the form of the computed I_{sc} from the regression method. However, to fully validate this method more data is needed, especially for comparison with other spectral reconstruction methods.

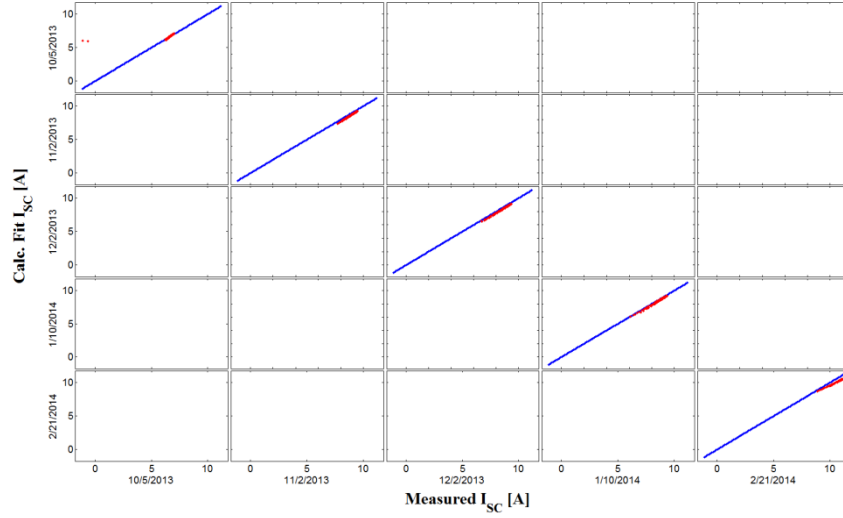


Figure 6. Regression between measured and predicted m-Si module I_{sc} using a regression method with seasonal interaction terms. The blue line provides a one-to-one correspondence reference while the red points are the respective data values for the five months.

A third method was also developed to reconstruct the solar spectrum from the five sensor measurements at discrete spectral bands. The processing for this method was more involved and uses the SMARTS2 (NREL) software. The atmospheric transmission will be developed analytically based on the measurements from the five photodiodes. Accurate modeling of the atmospheric transmission is highly dependent on the spectral bands over which the solar spectrum is sampled, whereby the analysis producing Table 2 will be utilized. The atmospheric components (e.g. aerosols, H_2O , ozone, and gasses) can be separated and monitored with the discrete spectral sensors. Using SMARTS2, the atmospheric transmission profiles can be constructed for the different atmospheric components based on the sensor measurements. A final transmission profile (that accounts for the atmospheric components) can be applied to the extraterrestrial solar spectrum to predict the spectrum on the ground using Eqn. 3:

$$E(\lambda) = E_0(\lambda) \cdot r^2 \cdot T_a(\lambda) \cdot T_g(\lambda) \cdot T_n(\lambda) \cdot T_o(\lambda) \cdot T_R(\lambda) \cdot T_w(\lambda) \quad (3)$$

where the subscripts 0, a, g, n, o, R and w correspond to extraterrestrial, aerosols, mixed gases, nitrogen, ozone, Rayleigh scattering, and water respectively. Figure 7 shows an example of a reconstructed solar spectrum from simulated sensor measurements compared to the solar spectrum measured with our spectroradiometer. This investigation developed novel algorithms that use non-linear optimization routines to model the transmission profiles for the different atmospheric components. Work is currently underway to refine this method to reduce uncertainty in the solar spectrum prediction. From the reconstructed solar spectrum the predicted module short-circuit current can then be computed.

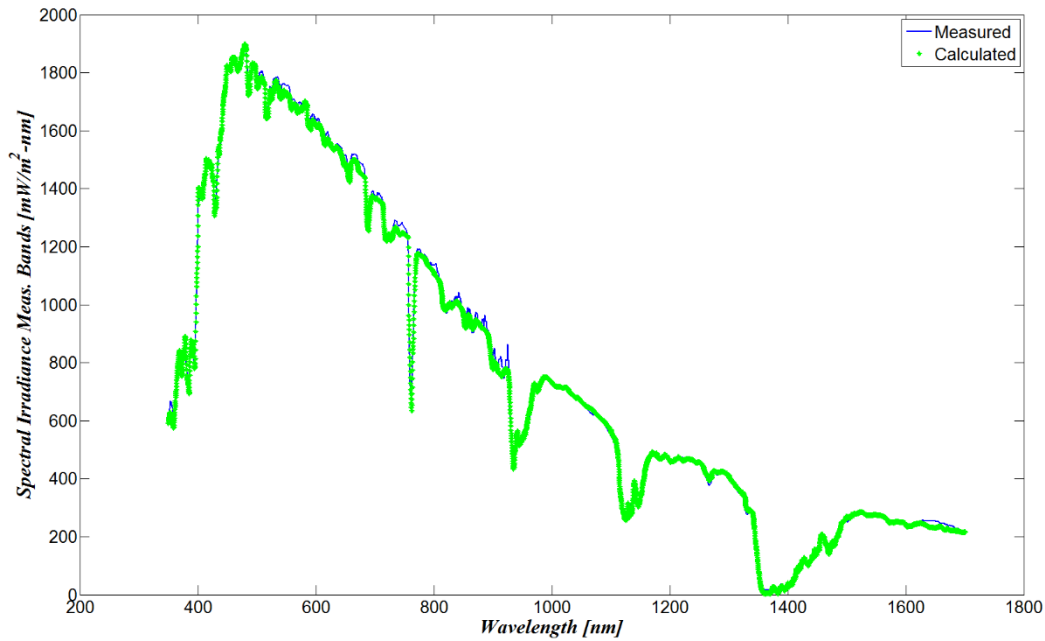


Figure 7. Solar spectral irradiance prediction model comparison with the measured c-Si module data.

Spectral data is currently being collected with our prototype spectral device. The individual sensors will be calibrated after sufficient data is collected. Once the sensors are calibrated, the post-processing algorithms will be applied to the sensor data. Continued refinement to the algorithms will be performed to reduce the uncertainties in the predictions. Additionally, any improvements that are made will be listed and recorded for the next iteration of the prototype. In particular, focus will be made to reduce the sensor complexity and material geometries, to reduce the overall cost. In addition to this current tracking sensor prototype, design work is also underway to develop a non-tracking spectral sensor, which will eliminate the need for an expensive two-axis tracker. A non-tracking sensor could be advantageous for PV plant facilities that do not have access to two-axis trackers. Because of the unique concept that the Sandia team has on the non-tracking sensor, a Technical Advance with Sandia will be submitted for a potential patent application.

3. RESULTS

After alignment of each of the photodiodes was completed, to ensure accurate current readings from each of the photodiodes with low signal noise, a preliminary gain settings analysis was performed. Here the sensors were setup on a two-axis tracker to record data under clear-sky conditions, around solar noon. Only a one minute delay occurred between each successive test to allow for an approximation of similar irradiance conditions. Data was recorded for one minute for each gain setting to determine which level allowed a signal-level buffer prior to the saturation limit. Each setting was also assessed to ensure the signal noise had good sensitivity without saturation. Figure 8 provides an example of the data recorded for the 630 nm photodiode sensor test where the 390 μ A gain setting proved to be most optimal.

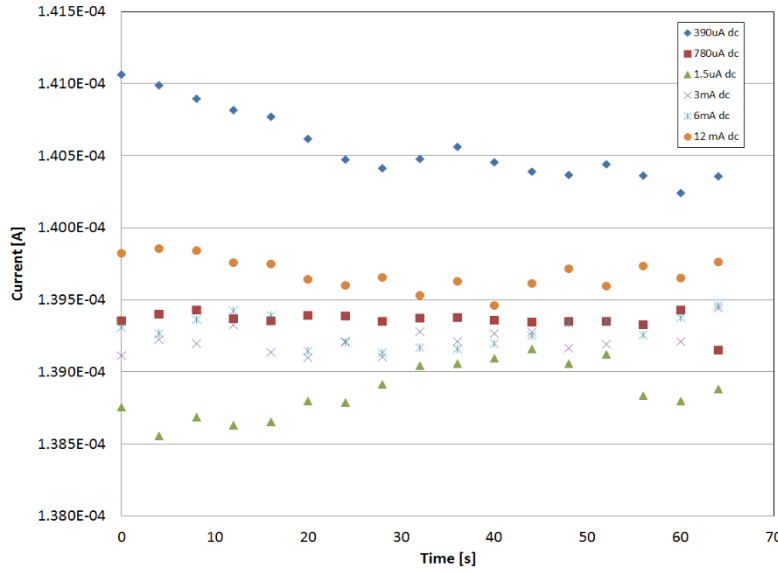


Figure 8. Photodiodes Gain Setting Optimization Analysis for the 630nm sensor.

Once the gain settings were optimized for maximum sensitivity for each of the photodiodes, a calibration set was then performed between each photodiode and the wide-band EKO spectrometers that were also mounted on the same two-axis tracker. For this calibration, a regression analysis was performed of the measured current data from each of the photodiodes against the measured in-band spectral irradiance, prescribed by Eqn. 4.

$$E = \int_{\lambda_c - \Delta\lambda/2}^{\lambda_c + \Delta\lambda/2} E_\lambda d\lambda \quad (4)$$

Figure 9 presents an example of this analysis for the 630 and 940 nm sensors where linear regression fits were employed. The fit functions are then used as correction functions. The signals from the sensor can be filtered through the correction functions to obtain the irradiance value for the sensor operating spectral band.

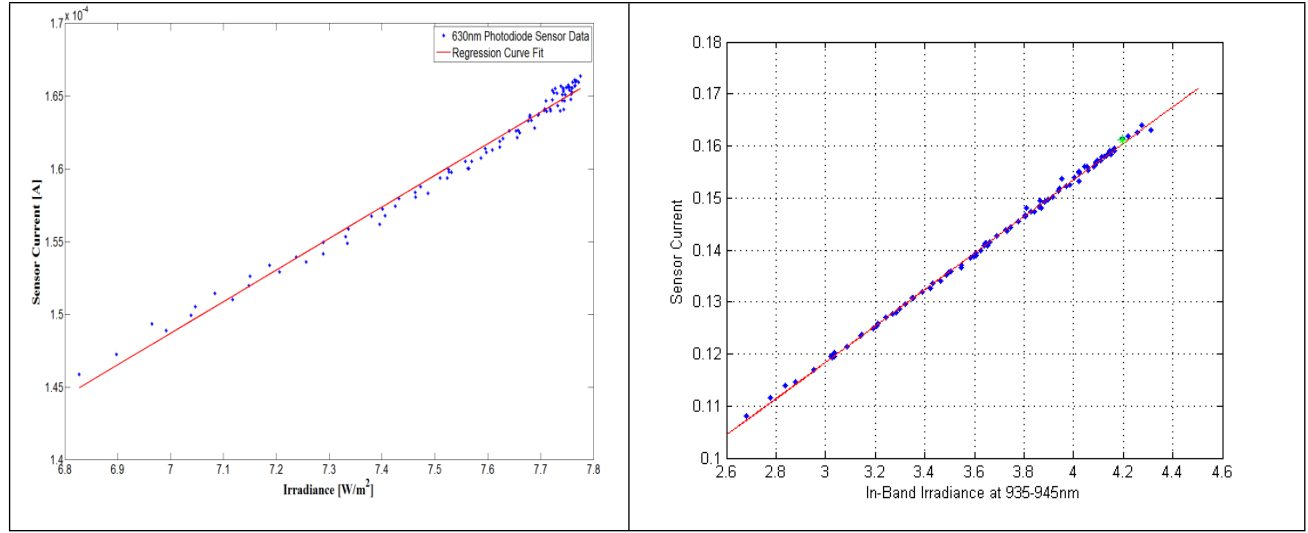


Figure 9. Photodiodes Sensor Calibration Analysis for the 630 nm and 940 nm sensors.

Using this calibrated data, measured photodiode data was compared against measured EKO wide-band spectral data from the PSEL spectrometers. Currently, the results shown in Fig. 10 suggest good correspondence, especially for the 500 nm, 580 nm, 630 nm and 940 nm bands; however more seasonal data is needed to validate this method.

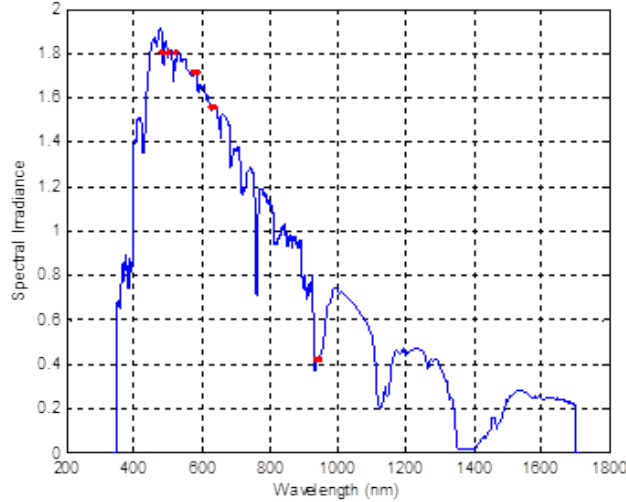


Figure 10. Calibrated photodiode measurements (red) of 500nm 580nm 630nm and 940nm bands, with EKO spectrometer data (blue).

For spectrum reconstruction, the method employed in this investigation utilized aspects of the SMARTS2 transmission model based on a condensed version of Eqn. 3:

$$E = r^2 T E_0, \quad (5)$$

where E is the measured irradiance, E_0 is the extraterrestrial irradiance (at AM_0 measured above the earth's atmosphere), T is the total atmospheric transmittance affected by attenuation through the atmosphere, and r is the ratio of the average to actual sun to earth distance. Fig. 11 presents a comparison of the extraterrestrial spectrum versus an example of the measured spectrum. Also included is a corresponding example of the transmittance distribution calculated from Eqn. 6.

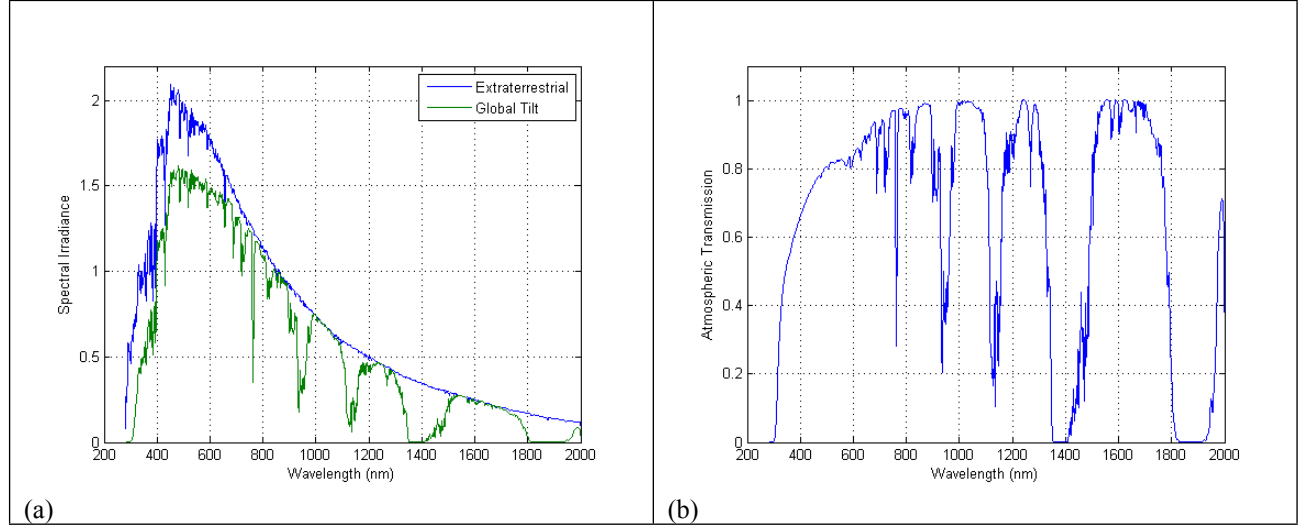


Figure 11. (a) Extraterrestrial and global tilt spectral irradiance (ASTM G-173). A ratio of the two curves in (a) provides the (b) transmittance through the atmosphere (from extraterrestrial to the ground).

The atmospheric transmittance can be estimated from the measured irradiance on the ground by:

$$T = \frac{E}{r^2 E_0}, \quad (6)$$

since the extraterrestrial irradiance is fairly constant anywhere above the atmosphere. The atmospheric attenuation is caused by aerosols, ozone, gases, water vapor, and Rayleigh scattering. Each constituent affects different parts of the spectrum. Equation 1 can be written as a function of the wavelength, in which case the quantities become spectral. The spectral irradiance is then defined as:

$$E(\lambda) = r^2 T(\lambda) E_0(\lambda). \quad (7)$$

By using the calibrated values of the photodiodes as well as the respective values of E_0 , according to Eqn. 6 we are then able to compute the respective transmission values as presented in Figure 12b.

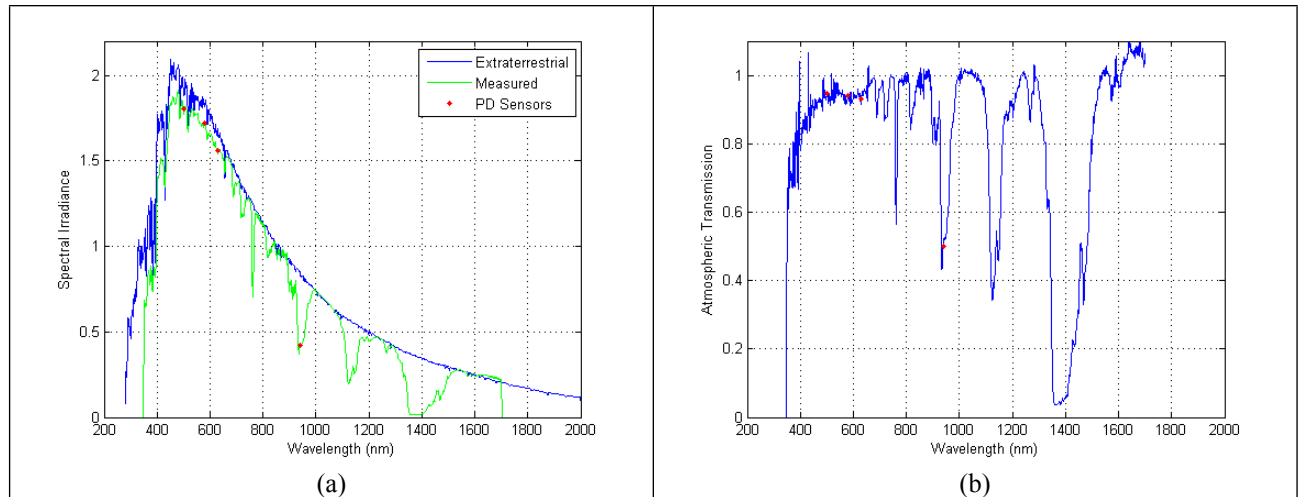


Figure 12. (a) Extraterrestrial spectral irradiance compared to the measured spectral irradiance at 11:40 am local time on Oct. 1, 2014 in Albuquerque, NM, and the data from the calibrated spectral sensors (red dots) for the same day and time. (b) Transmittance profile of the measured spectral irradiance shown in (a) and the corresponding calculated transmittance from the PD spectral sensors (red dots). Note that the r^2 factor was not accounted for in the calculation.

Using this calibrated data, each of these transmission points were then used to optimize, and compute the spectrum according to their respective time series values. This functionality was built into the novel Sandia Spectral Transmission Model, to compute the spectrum based on fundamental atmospheric physics. Once the optimization routine was completed the spectrum was calculated and compared to the spectral irradiance measured by the wide-band EKO spectrometers. As shown in Figure 13 at solar noon on October 1, 2014, the reconstructed spectrum had a close correspondence with the full-band measured spectrum with an RMS error of 38.2.

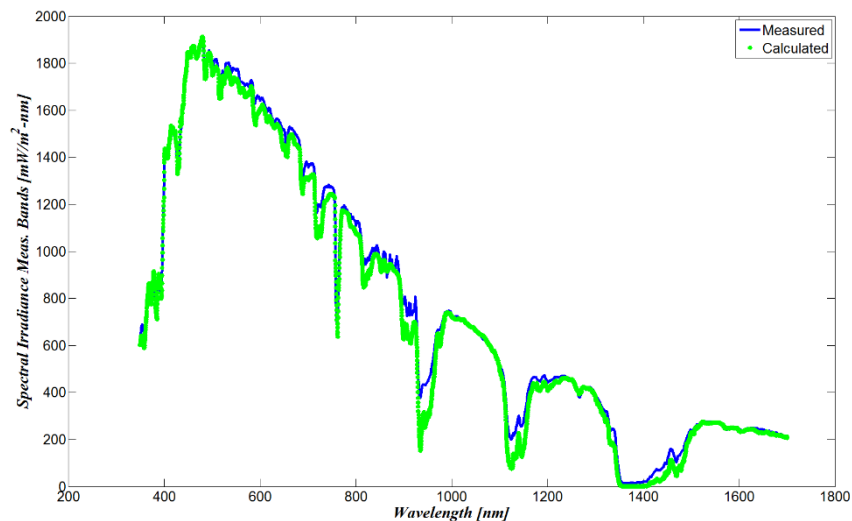


Figure 13. Calculated spectrum based on discrete photodiode measurements and computation within the Sandia Spectral Transmission Model, compared with measured full-band spectrum from an EKO spectrometer for October 1, 2014.

Next, using this data with Eqn. 2 we are able to compare the calculated short circuit current. From Figure 14, the results suggest close agreement to within an RMS error of 0.05 A. Work will continue to improve on spectrum reconstruction to reduce the uncertainty when compared to the measured spectrum.

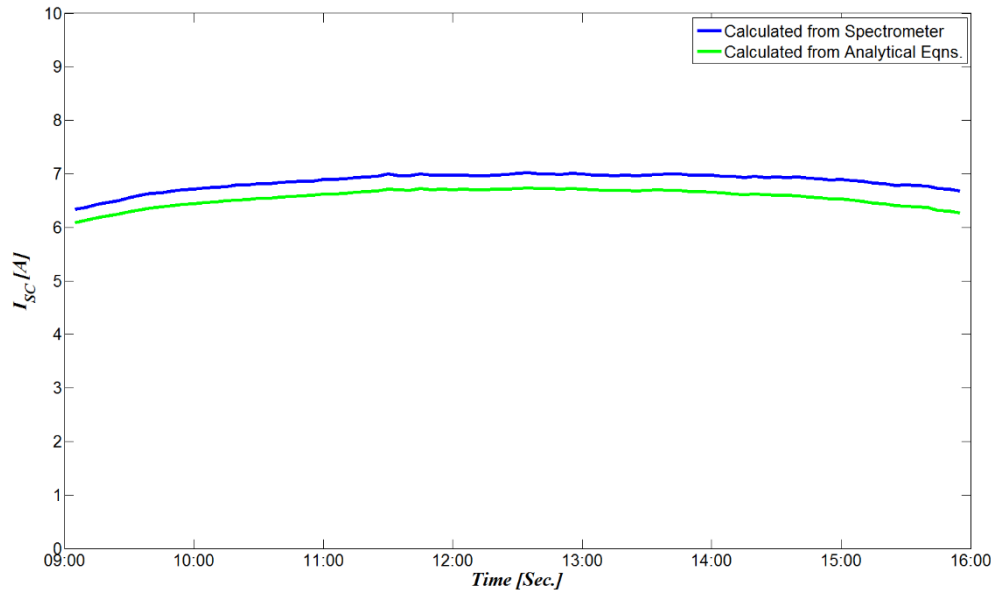


Figure 14. Comparison of short circuit current between EKO spectrometer and measured photodiode data with spectral reconstruction using the Sandia Spectral Transmission Model, for October 1, 2014.

4. CONCLUSIONS

Spectral information for a PV site is critical for optimized electrical generation performance with respect to the spectral response of a particular module technology. However, the spectral data for all parts of the US (and globally) is limited due to mostly to costs [1] for spectrometer equipment. In this investigation a novel low-cost, discrete-band sensor device, comprised of five narrow-band sensors, was developed for ubiquitous adoption for PV site measurements and predictive performance modeling. In this work, two I_{sc} prediction methods were developed based on an interaction-terms regression methodology, as well as a spectrum reconstruction methodology for computing I_{sc} . The results of this work found for the spectrum reconstruction method computed spectrum were close within an RMS error of 38.2 W/m²-nm. Further analysis of computed I_{sc} found a notably close correspondence of only 0.05 A RMS error. However, more data collection is needed for validation of this method, as well as the interaction-terms method, with experimental module data.

5. REFERENCES

1. K.M. Armijo, R.K. Harrison, B.H. King and J.B. Martin, "Spectral Derates Pheonomena of Atmospheric Components on Multi-Junction CPV Technologies," *10th International Conference on Concentrator Photovoltaic Systems*, Albuquerque, NM, 2014.

APPENDIX A: SILICON PHOTODIODES

Thorlabs silicon photodiodes are ideal for measuring both pulsed and continuous-wave fiber light with sensitivity from 340 to 1100 nm. An image of the photodiode and its specifications are shown in Figure #. The detector is housed in a ceramic package with anode and cathode connections. Under reverse bias applications, the photodiode anode produces a current, which is a function of the incident light power and wavelength. The responsivity of the photodiode is used to estimate the amount of photocurrent per incident light energy. The photo current can be converted to a voltage by placing a load resistor between the photodiode anode and the circuit ground. The bandwidth and rise time response are determined from the diode capacitance and the load resistance. The diode capacitance can be lowered by placing a bias voltage from the photodiode cathode to the circuit ground.



Specifications

Specification		Value
Wavelength Range	λ	340 - 1100 nm
Peak Wavelength	λ_p	960 nm
Responsivity	$R(\lambda_p)$	0.62 A/W
Active Area		100 mm ²
Rise/Fall Time ($R_L=50 \Omega$, 5 V)	t_r/t_f	150 ns / 150 ns
NEP, Typical (960 nm)	W//Hz	1.50×10^{-14}
Dark Current (5 V)	I_d	200 pA
Capacitance (5 V)	C_j	380 pF
Package		Ceramic
Sensor Material		Silicon (Si)
Maximum Rating		
Max Bias (Reverse) Voltage		5 V
Operating Temperature		-40 to +75 °C
Storage Temperature		-55 to +125 °C

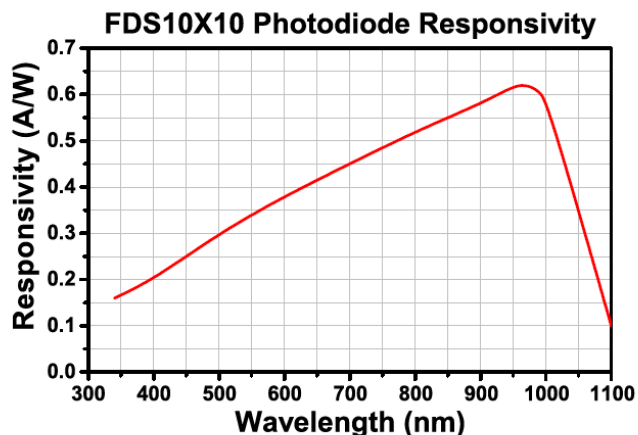


Figure A1. Thorlabs silicon photodiode, its specifications, and typical responsivity curve.

APPENDIX B: SPECTRAL BANDPASS FILTERS

Thorlabs Laser Line and Bandpass filters provide a simple and economical way to transmit a light in a narrow, well-defined spectral region while rejecting other unwanted radiation. Their design is essentially that of a thin film Fabry-Perot Interferometer formed by vacuum deposition techniques and consists of two reflecting stacks, separated by an even-order spacer layer. These reflecting stacks are constructed from alternating layers of high and low refractive index materials, which can have a reflectance in excess of 99.99%. By varying the thickness of the spacer layer and/or the number of reflecting layers, the central wavelength and bandwidth of the filter can be altered. This type of filter displays very high transmission in the bandpass region, but the spectral range of blocked light on either side of the bandpass region is narrow. To compensate for this deficiency, an additional blocking component is added, which is either an all-dielectric or a metal-dielectric depending on the requirements of the filter. Although this additional blocking component will eliminate any unwanted out-of-band radiation, it also reduces the filter's overall transmission throughput. Using these methods, Thorlabs offers a wide range of filters from 340 nm - 1650 nm. In addition, custom filters can be fabricated.

An example of a filter is shown in Figure # (for the 940 nm with a bandwidth of 10 nm).

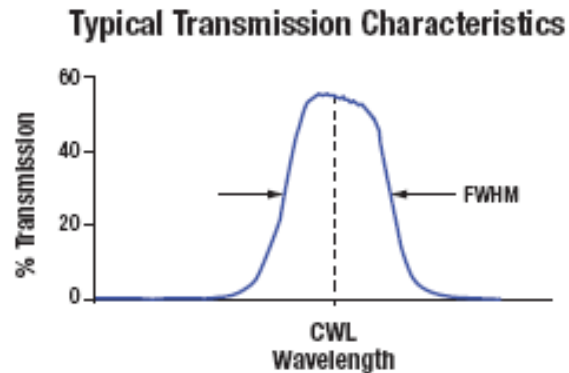


Figure A2. Example of a Thorlabs bandpass filter, and a typical transmission profile for the bandpass filters.

